

Photophysical properties of materials for high-speed photodetection

Amin Morteza Najarian¹, Maral Vafaie¹, Bin Chen², F. Pelayo García de Arquer³ & Edward H. Sargent^{1,2,4}✉

Abstract

Fast-response optical sensing across the electromagnetic spectrum is an enabler of quantum systems, 3D machine vision and augmented reality, yet existing technologies are not optimized for infrared sensing. Trade-offs among characteristics such as speed, efficiency, noise, spectral detection range and cost motivate the research community to develop nanostructured sensing materials that provide operation from visible to infrared wavelengths with seamless integration. As efforts are made to advance the combined gain and bandwidth of devices, a clear understanding of physical mechanisms underlying the dynamics of charge carriers, with a particular focus on speed-limiting processes, is of high priority. In this Review, we provide an account of the photophysical attributes of active materials and their impact on optical sensor performance, focusing on the interplay between temporal and peak response to pulsed light of varying durations. We identify performance-limiting processes and directions for future progress in developing materials and device architectures that realize high-speed photodetection.

Sections

Introduction

Peak response

Response time

Recovery time

Outlook and direction of development

¹The Edward S. Rogers Department of Electrical and Computer Engineering, University of Toronto, Toronto, Ontario, Canada. ²Department of Chemistry, Northwestern University, Evanston, IL, USA. ³ICFO — Institut de Ciències Fotòniques, The Barcelona Institute of Science and Technology, Barcelona, Spain. ⁴Department of Electrical and Computer Engineering, Northwestern University, Evanston, IL, USA. ✉e-mail: ted.sargent@northwestern.edu

Key points

- The dark-current–speed–efficiency triangle, a principal performance measure for photodetectors, now places a higher emphasis on detection bandwidth, a key metric for a range of emerging applications.
- In pulsed detection, unlike continuous light detection, the peak response depends on the photodetector's response time; a slower detector results in a reduced peak response.
- Response and recovery time represent distinct aspects of speed within the characteristics of a photodetector. They originate from the intricate relationship between photophysical properties, affecting the temporal dynamics of charge-carrier transport and collection.
- Transport and capacitance are the main limiting regimes for response time, mainly determined by the mobility of charge carriers and the dielectric constant of the active material.
- Improvement of recovery time requires a detailed investigation of the sources of charge trap states, characterized by their energy depth, distribution and total density.

Introduction

Optoelectronic applications are continuously evolving toward faster operation with higher resolution and accuracy. This has led to growing demand for fast photon-to-electron transduction. The advance of high-speed optical sensing has contributed to telecommunications¹, quantum technologies^{2–4} and consumer electronics^{5,6}. In particular, fast and efficient photodetectors are essential elements in technology that uses lidar (light detection and ranging). In a lidar system, photodetectors convert backscattered light from the targeted object into electrical signals, which are then used to determine distance. Fast and sensitive photodetection is important in this context to provide accurate spatial resolution over long distances⁷.

Although silicon-based photodetectors are an established technology, they have shown only limited sensitivity at wavelengths longer than 1,000 nm (refs. 5,8–11); for this reason, alternative material systems have been explored over the past 30 years. The best-performing fast infrared-sensing technologies rely on epitaxially grown materials, notorious for their low yield and costly scale-up and integration. Solution-processable materials including organics^{12–16}, colloidal quantum dots^{17–19}, perovskites²⁰ and 2D materials^{21–23} stand out as potential solutions, providing a means to exploit the relationship between structure, property and function^{12,18,20,24–26}.

In addition to developing fast infrared sensors, it is necessary to consider compatibility with silicon for integrated devices, such as complementary metal–oxide–semiconductor technologies and silicon-on-insulator. Factors that affect the integration process include materials processing compatibility, interfacial quality, energy-level alignment, stability and encapsulation. Additionally, photodetectors can be used in photonic integrated circuits, where the higher speed of optical processing compared with conventional electronic counterparts enables faster operation. These on-chip circuits allow for single-photon operations, which are gaining traction in quantum technologies including metrology, computing, communication and information processing^{4,27–30}. The single-photon detectors must meet

specific criteria for fidelity, including high sensitivity, low jitter and fast response. Their hybrid on-chip integration will benefit from innovation in materials, architectures and detection mechanisms^{29,31,32}.

In this Review, we discuss the photophysical properties of photodetectors. Often, the quantum efficiency of photodetectors is measured by using continuous illumination. Continuous light detection involves the steady-state conversion of a continuous-wave stream of impinging photons into electrical signals, a task that primarily emphasizes the photodetector's responsivity and noise characteristics, but overlooks the role of speed in determining peak response (amplitude). Pulsed or modulated light detection involves dealing with temporally evolving light signals, placing a premium on the speed and bandwidth of the photodetector. Here we focus on the case of pulsed light, discussing the interplay between the distinct characteristics of speed (rise, fall and recovery time) and the efficiency of photodetectors in determining the peak response. We place emphasis on how the photophysical properties of active materials affect their maximum achievable combined gain–speed characteristics (Fig. 1).

Following an introduction to the elements of photodetector architecture and operation, we discuss device-level variables, including geometric area, external bias, material thickness and light exposure duration. These factors allow evaluation of the origins of limitations on device speed. This approach enables iterative device design and can be further refined by characterization methods that probe materials-level properties for fast photodetection, such as charge carrier mobility, lifetime and dielectric constant. These inform models of device performance, and they can influence device architecture. Looking beyond photodetectors, we discuss carrier dynamics in response to pulsed light, as this offers insight into the physics of optoelectronic systems such as solar cells, light-emitting diodes and lasers. For example, although solar cell output may not be directly affected by rapid response to fluctuations in light intensity, analysing their transient response provides information on photoexcited charges in the full stack devices^{33–35}. We conclude by offering a perspective on the future of the field.

Peak response

External quantum efficiency (EQE, η_e) measures the efficiency of photodetectors and photosensitive devices in converting incident photons into electrical signals. In the context of pulsed light, EQE can be determined as the ratio of collected charge carriers to the total number of incident photons during a single light pulse ($\eta_e = N_c/N_p$). The total number of incident photons (N_p) is calibrated by using an external photodetector with a known response, integrating the resulting photoreponse and considering the illuminated area (Fig. 2a). The number of collected charge carriers (N_c) is measured from the output of the photodetector versus time, using similar illuminating conditions (Fig. 2b). Synchronization of measurements to account for different timescales between light duration and detector response is essential for accurate EQE calculations. Averaging multiple pulse measurements can provide a more statistically meaningful representation of the overall EQE.

The peak response is the maximum measurable output signal produced by the photodetector in response to a single pulse of light. Considering the above definition of EQE, when the light duration is shorter than the detector's response time, the PR is a function of EQE, light duration and response time of the photodetector. Figure 2c illustrates the responses of three photodetectors, each with differing speeds, to a single light pulse of similar power and duration. Although these photodetectors have the same EQE – as seen in the integral of the area beneath their peak responses – the graph shows that a detector

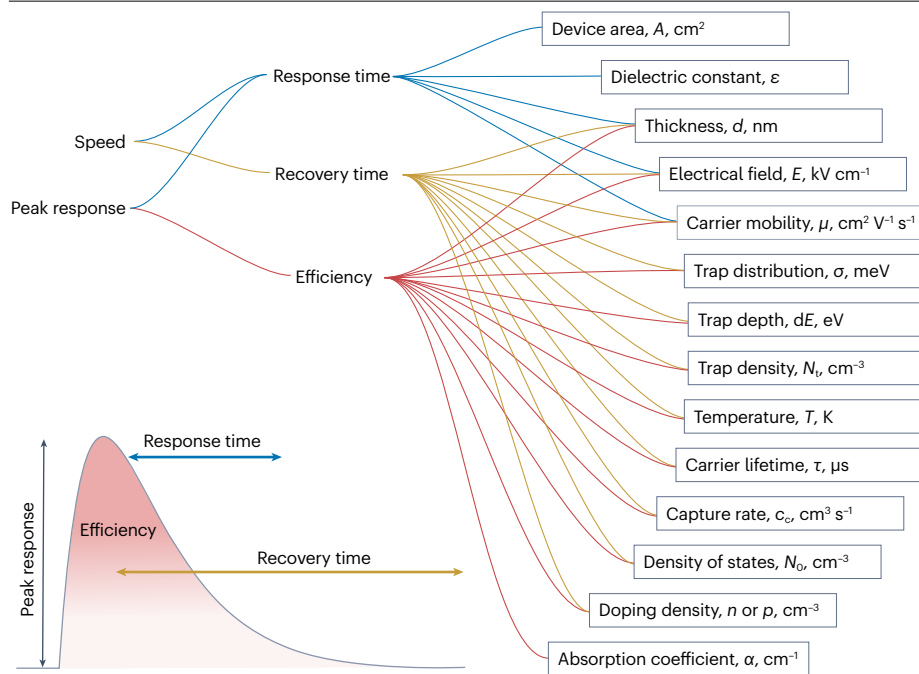


Fig. 1 | Connections between the performance of photodetectors and the photophysical characteristics of electronic materials. The peak response of photodetectors is intricately linked to both the speed and efficiency of detection, which are governed by the complex relationship between the material's photophysical properties.

with a slower response time yields a diminished peak response. By assuming an exponential rise and decay for the current, we propose that the peak response can be estimated as $n_e/2.2(\tau_f + \tau_r)$. We discuss later that τ_r can itself be a function of light duration.

To understand the effect of speed on the peak response and its relevance to the light duration, we introduce the maximum achievable peak response (MAPR) metric. The MAPR of a photodetector is defined as its peak response to a short light pulse divided by peak response to continuous light, but only when the peak power of the light pulse is equal to the average power of the continuous light. Figure 2d shows MAPR as a function of both light duration and the photodetector's response time. Ideally, the MAPR should approach 1.0 for the most effective performance (maximum sensitivity). This condition is met when the response time of the photodetector is comparable to or faster than the light duration.

The case of modulated light

In scenarios involving modulated light, the peak-to-peak response of a photodetector is influenced by its speed, particularly when its bandwidth does not fully encompass the frequency of the incoming light. Figure 2e demonstrates this by showing the responses of three photodetectors, differing in speed but identical in efficiency, to sinusoidally modulated light. Notably, detectors with slower response times have reduced peak-to-peak responses and a phase shift. It is important to note that the average response remains unaffected by the photodetector's speed.

The use of a photodetector with a limited bandwidth further complicates the matter in at least two ways. The first is a phase shift between the incident light and the recorded signal. The second is the appearance of spurious signals at frequencies that deviate from the fundamental frequency, leading to frequency impurity. This is observed when the detected signal deviates from an ideally symmetric, perfect sinusoidal shape.

Other light waveforms, such as triangular ones, and modulations, such as amplitude modulation, are used for specific functions and applications. Despite their differences, they conform to the same underlying principles of photodetection: for optimal performance, the response time of the photodetector should be faster than the light modulation frequency or pulse duration.

Combined gain–bandwidth characteristics

Gain is an important factor in defining the sensitivity of the detector in response to continuous light. Under pulsed illumination, however, a detector with a higher gain may not translate to a higher peak response or signal-to-noise ratio (Box 1). For example, in photoconductors, the gain is realized through the repeated circulation of free carriers across the device. If we define τ_1 as the time required for a carrier to complete one full transit across the device, the total response time can be approximated as $\text{gain} \times \tau_1$.

A trade-off can arise wherein higher gain results in a decrease in speed (Fig. 2f), which shows the impact of gain on response time. The figure includes several lines representing different photoconductors, each marked with a specific τ_1 value (the transit time of the carrier for one cycle), ranging from 1 ps to 1 μs. A photoconductor with a given transit time can attain high gain, but this comes at the expense of speed. Because the peak response is dependent on speed, this gain mechanism does not enhance the achievable peak response: indeed, it may lead to increased levels of dark current and noise. Photodiodes, which ideally do not incorporate a gain mechanism, can achieve a wide spectrum of speeds independent of their efficiency. This is represented by a horizontal line in the graph.

Response time

The response time is defined as the duration of the rise (τ_r) or fall (τ_f) of the detector's output signal, typically in the range of 10–90% of its peak response, and has implications for application-specific

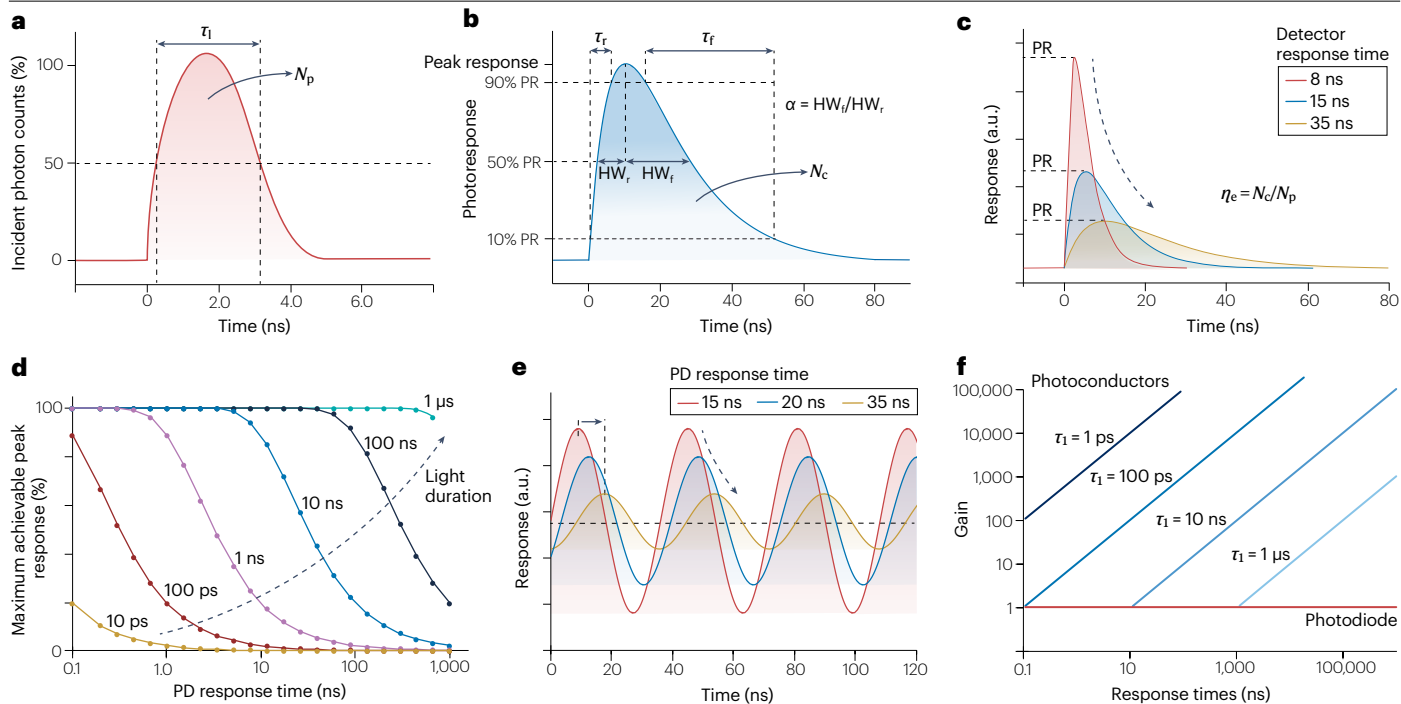


Fig. 2 | PR in pulsed light detection. **a**, Plot of number of photons N_p versus time for the incident light. The area under the plot represents the total number of received photons. Pulse duration τ_i is defined as the full width at half maximum of the pulse. **b**, Output of photodetector plotted as current versus time. The area under the plot represents the total number of collected charges N_c . HW_r and HW_f are half-width during signal rise and fall, respectively. **c**, Simulated response of a photodetector (PD) with the same external quantum efficiency (η_e) but different response times (8, 15 and 35 ns) to the 1-ns light pulse. **d**, Calculated maximum

achievable peak response (MAPR) versus response time of a photodetector for a range of indicated light pulse duration. MAPR is defined as the peak response (PR) magnitude of the photodetector in response to a light pulse divided by the response to a continuous light with the same peak power. **e**, Simulated response of a photodetector with different response times to the same modulated light at a frequency of 25 MHz. **f**, The calculated maximum gain of a photodetector versus its response time. τ_i represents the transit time of the carrier for one cycle.

performance metrics such as lidar distance resolution. This is because the algorithms, or methods, used to transform temporal data into spatial information require sharp peaks and minimal phase delay, jitter and frequency impurities.

As detectors reach faster response times at the nanosecond level, the use of high-bandwidth oscilloscopes, along with the limitations of current amplifiers and the difficulties in focusing infrared pulsed light on small detector pixels, increases the noise level. This complexity challenges the accuracy and consistency of measuring the detector's response time at 10% of its peak response²⁰. Although curve fitting is beneficial, it may lead to inconsistencies in reports due to the varied functions and methods used. We propose that examining the half-widths at the half-peak response (Fig. 2b) offers a more reliable metric for comparison across studies than measuring response time at 10% of peak, which can be near the noise threshold of measurements: the half-width during signal rise (HW_r) and that during fall (HW_f). We also can define a symmetry factor, α , as $\alpha = HW_r/HW_f$. Later, we discuss how this factor deviates from 1.0 (perfectly symmetric) as the light pulses become shorter than the photodetector's response time.

Capacitance-limited response time

The dynamics of charge-carrier separation and transport are noticeably affected by electrostatic effects, such as capacitive charging, which are influenced by the dielectric properties of the different layers and

interfaces present in the photodetector^{18,20,36–38}. This introduces a lag phase before achieving equilibrium, ultimately defining the upper limit of a photodetector's response time. The main factor contributing to this limitation is the capacitance of the active layer. In a fully depleted system, the RC-limited response time can be quantitatively described by the following equation:

$$\tau_{RC} = 2.2RA\epsilon_r\epsilon_0/d \quad (1)$$

Here, ϵ_r denotes the dielectric constant, ϵ_0 the permittivity of free space, A the effective area of the device, and d the material's thickness. Figure 3a plots the response time of a photodetector as a function of thickness for a range of dielectric constants between 10 and 55 (representative of typical semiconductor materials). In the capacitance-limited regime, response time has a direct relationship with thickness. It is important to recognize that interfacial capacitance in a device's layered stack can contribute to the overall capacitance. To measure and characterize these capacitance components and spatial charge effects properly under pulsed light, advanced impedance spectroscopy and modelling are required^{35,38–41}.

Transport-limited response time

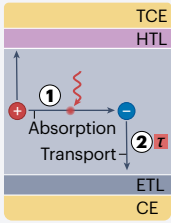
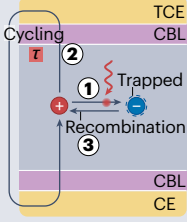
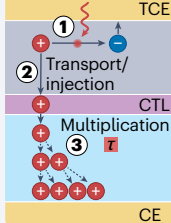
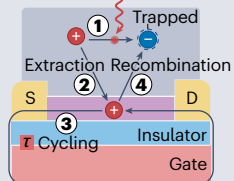
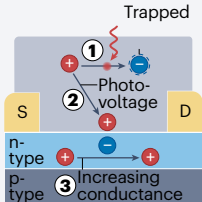
Following the production of electron–hole pairs in the absorbing layer, the time it takes for a free charge carrier to cross the device is

Box 1

Photodetector architecture

The process of photodetection consists of sequential steps, involving photon absorption, photon-to-charge conversion leading to an electron–hole pair, and subsequent carrier separation, transport

and extraction. This process can be implemented in different device architectures (Table), leading to different operating principles and performance.

Architecture	Gain	Speed	Dark noise	External bias (V)	Development stage	Cost	Research focus	Comment
Photodiode 	No gain	Fast, >40GHz	Low	0–5	Mature	Low	Active materials for extended detection spectrum Seamless integration with developed readout circuits and integrated photonic platforms	The most studied and reliable architecture with the fastest response time Usually designed as n–i–p or p–i–n architectures
Photoconductor 	1–10 ⁶	Slow, <1MHz	Moderate to high	1–30	Developing/mature	Low	Rational combined gain–bandwidth	Response time is dictated by the lifetime of trapped carriers Gain is voltage-dependent Larger gain often results in extended response time and an increase in dark current
Avalanche photodiode 	5–10 ⁶	Moderate to fast, <1GHz	Moderate to high	5–200	Mature	Moderate–high	Fast response with advanced quenching mechanism New multiplier/absorbing material pairs Scale-up yields, high pixel density, larger area	Operation in Geiger mode enables single-photon detection Silicon and InGaAs are extensively used in these architectures Yields are limited in the production of these architectures with large area
Hybrid photo-FET 	1–10 ⁵	Moderate, <10MHz	High	1–50	Developing	Moderate	Interface engineering for efficient and selective carrier extraction Justified trade-off between dark signal and speed Transport materials with high mobility	Multiplication is decoupled from the light absorption Speed is primarily defined by the mobility in the transport layer
Photovoltage FET 	1–10 ⁵	Moderate, <10MHz	Moderate to high	1–50	Proof of principle	Moderate	Studying operation mechanism Exploring the limits Tuning channel transduction Maximizing short-lived interfacial photovoltage	The mechanism relies on the generated photovoltage at the interface, which regulates the transduction in the underlying PN channel The speed might be dictated by the lifetime of the carriers accumulated at the interface

τ, step that usually determines speed; CBL, charge-blocking layer; CE, conductive electrode; CTL, charge transport layer; ETL, electron transport layer; FET, field-effect transistor; HTL, hole transport layer; TCE, transparent conductive electrode.

(continued from previous page)

Photodiode. In this configuration, the active layer is positioned between two charge-selective transport layers, commonly in an n-i-p or p-i-n arrangement. Electrons and holes are extracted through the charge-selective contacts via drift (built-in and applied electric field, if any) and diffusion. In this design, the response time is determined by the transit time of carriers across the junction and extracting layers, as well as by capacitive effects from interfaces, depleted and quasineutral regions^{91,92}.

Photoconductor. In this architecture, the active layer is between charge-selective layers, typically incorporating metals whose work function aligns with the semiconductor's Fermi level. Photoexcitation leads to the retention of minority carriers in the active layer — either through capture in trap states or due to their inherently lower mobility or blockage of injection to charge-selective layers — whereas majority carriers circulate multiple times under the applied bias until they recombine with the minority carriers^{15,32,49,91,93}. Consequently, the response time is predominantly governed by either the trap lifetime or the mobility disparity between minority and majority carriers. This design offers a bias-dependent gain attributable to carrier recirculation, quantified as the ratio of the trapped carrier lifetime to the transit time of the majority carriers across the device.

Avalanche photodiode. This architecture builds on a photodiode configuration especially designed to sustain high electric fields combining highly doped and intrinsic layers. Photoexcited carriers are swept based on the applied bias and then selectively injected into a multiplication layer. The distribution of applied electric field across the devices should be determined by modelling and needs

careful consideration for optimum results^{94–97}. Amplification, through secondary photomultiplicative gain, occurs based on charge scattering and impact ionization. When operated beyond the breakdown threshold voltage (known as Geiger mode), this architecture can achieve sufficiently high gain to enable single-photon detection, operating in a photon-counting mode that incorporates avalanche quenching mechanisms.

Hybrid photo-field-effect transistor. This design builds on the operating principles of a photoconductor, but achieves more degrees of freedom due to different, gate-tunable, transport and charge-trapping mechanisms. Typically, this architecture involves a photoabsorbing layer and a high-mobility charge transport layer. On electron-hole pair generation, one carrier is selectively extracted to the transport layer, where it circulates multiple times, driven by an applied source-drain bias^{32,98}. Charge recombination is prevented by a built-in electric field between the transport and absorbing layers. The gain mechanism is governed by the characteristics of the transport layer and the junction; both of which can be tuned through a gate.

Photovoltage field-effect transistor. In this hybrid configuration, the absorbing layer modulates a charge transport layer through electrostatic effects (akin to a junction-gate field-effect transistor)^{99–101}. On photoexcitation, a photovoltage at their interface serves as a gate that can close or open transport in the transport layer. Distinct from other gain-enabling designs, this architecture does not rely on the transport of photogenerated carriers to the transport layer, thus resulting in different device physics, and trade-offs in gain versus time response that are largely determined by the photovoltage dynamics.

called the time-of-flight or transit time (τ). To evaluate the time response, we commonly make several simplifying assumptions: that there is a uniform electric field and light absorption across the semiconductor, that drift is the main mode of carrier transport (negligible contribution from diffusion), especially in thin materials (<500 nm) under a constant external bias, and that carrier mobility is constant, with minimal effects from scattering or temperature gradients. With these assumptions, the averaged transit time (τ_{tr}) can be calculated using the formula $t_{tr} = d^2/\mu V$, where μ is mobility, d thickness and V bias (external plus built-in field). Figure 3b plots the response time of a photodetector as a function of thickness for a range of mobility between 0.001 and 0.1 cm² V⁻¹ s⁻¹. Thickness has a negative impact on the speed when the carrier transport is a limitation.

The interplay of capacitance and charge transport

The effect of thickness on speed depends on whether the device is limited by transport or by capacitance. A certain thickness range can be identified for which the total response time, τ_{total} , reaches a minimum (Fig. 3b)

$$\tau_{total} = \sqrt{(2.2RA\epsilon_r\epsilon_0/d)^2 + (d^2/\mu V)^2} \quad (2)$$

The determination of the optimal thickness involves various factors, such as mobility and dielectric constant, and can be estimated as $d_{opt} \sim \sqrt[3]{RA\epsilon_r\epsilon_0\mu V}$. Practically, it is important that the optimal

thickness falls within a range that ensures sufficient light absorption, considering the absorption coefficient (α) of the active layer (Fig. 3d): absorbed % = $100 \times [1 - e^{-\alpha d}]$ (in the case of single-pass absorption — that is, no reflection at the back electrode). Figure 3d presents a plot of the EQE over response time (representative of peak response) against material thickness for a selection of absorption coefficients. Peak response (EQE/response time) finds its optimum point at a specific thickness, and its magnitude is affected by the absorption coefficient. In the process of optimizing thickness for speed, it is important to ensure that the internal quantum efficiency (IQE) is not compromised, as excessive carrier recombination can occur in thicker materials. Therefore, the selection of thickness must be carefully evaluated, accounting for the trade-off between efficiency and response time, while being aligned with the specific needs of the targeted application.

Device area as a diagnosis tool

Assessing the limiting aspects of the time response of the photodetector is needed to improve its performance. At a first approximation, this involves identifying the roles of capacitance and transport effects. In this context, thickness and device area are valuable variables to interrogate device performance, given their different impact on transport and capacitance. For example, an analysis of response time versus device area provides a clear distinction between these two speed-limiting regimes^{20,25} (Fig. 3d). Although reducing the device area

Review article

can improve performance in systems with high dielectric constants and impedance, there are practical limitations. Using pixels smaller than a certain size may not be feasible for some applications. Additionally, if the illumination area is larger than the pixel area, lateral diffusion currents can contribute to the time traces, extending response times and complicating data interpretation.

Deviation of fall time from rise time

In circumstances where the light excitation is shorter than the response time, the rise time becomes a function of light duration (in contrast to the fall time). This is a consequence of the photodetector not reaching a steady state before the discontinuation of light. For short-pulse light, it is observed that the rise time of the response is comparable to the light pulse duration. By contrast, the fall time is independent of the light pulse duration. This results in asymmetric responses characterized by a fast rise and a slower fall. Figure 3f quantifies this effect by plotting the calculated ratio of the fall time to the rise time as a function of the light pulse duration for photodetectors with specified response times. This relationship offers a practical use: the duration of the light pulse can be estimated by comparing the fall and rise times of the response. It is important to note that for ultrashort pulse light (less than 100 ps), the measured rise time is often dictated

by the upper bandwidth of the measurement setup, such as the oscilloscope and amplifier.

Recovery time

The recovery time, often termed lag or relaxation time, denotes the time required for a photodetector to revert to its baseline state after excitation. In some cases, the accepted baseline is application-specific, referring to decay within a given percentage from the peak value, such as baseline <1% of peak value (Fig. 4a). This metric is crucial for imaging systems, especially when scene brightness undergoes substantial fluctuations, resulting in a shadowing or carry-over effect on transitioning from a luminous to a dim scene. In lidar applications, recovery time constrains both the repetition frequency and dynamic distance resolution. Excessive recovery times contribute to the cumulative build-up of dark current and noise, decreasing the overall signal-to-noise ratio. Accurate measurement of noise level and detectivity estimation of the infrared detector presents challenges that require meticulous attention^{42,43}.

Effect of defects on transport and electrostatic characteristics

Typically, material defects (such as vacancies, dangling bonds and grain boundaries) result in localized electronic states (traps) that negatively affect the dynamics of charge-carrier transport and recombination.

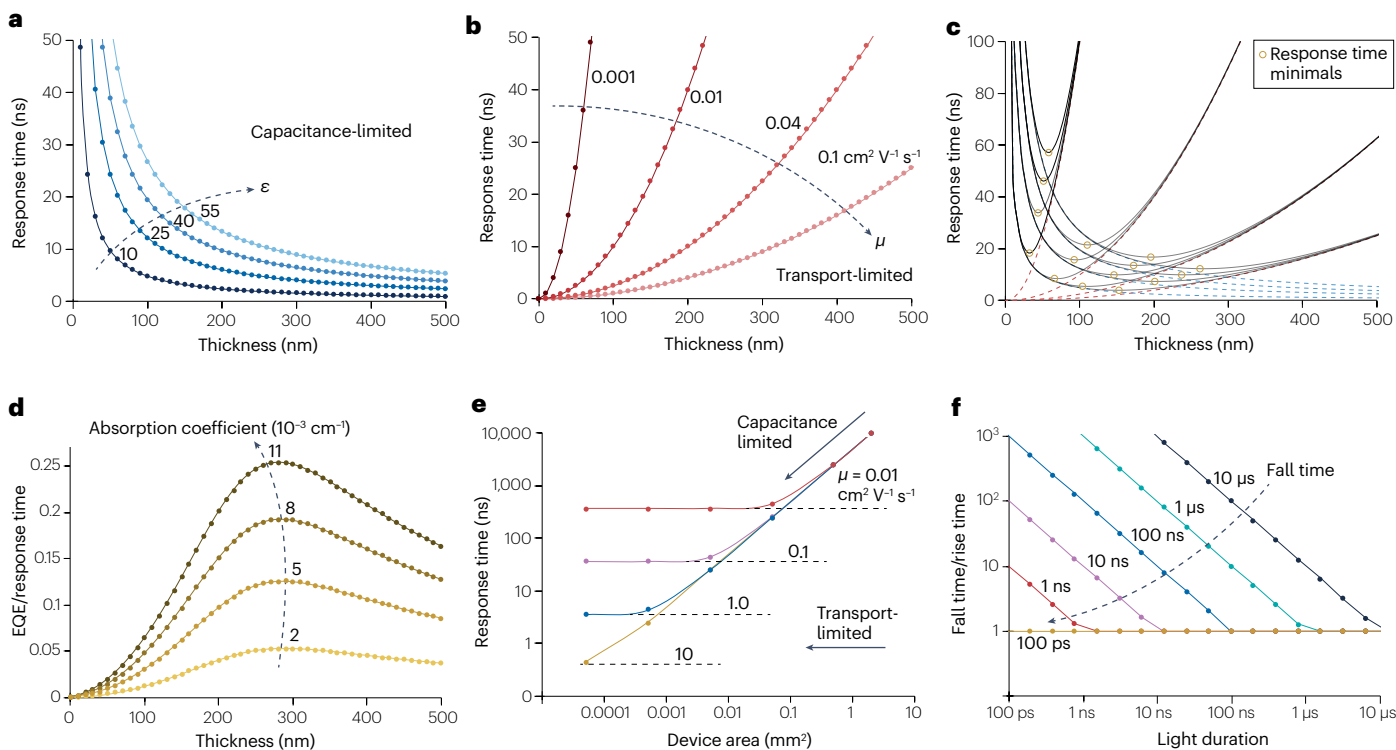


Fig. 3 | Transport-limited versus capacitance-limited response time. **a**, Plot of response time versus thickness, considering a range of dielectric constant ϵ from 10 to 55. For this modelling, the transport limitation is not considered. **b**, Plot of response time versus thickness, considering a range of mobilities μ from 0.001 to $0.1 \text{ cm}^2 \text{ V}^{-1} \text{ s}^{-1}$. For this modelling, the contribution from capacitance is not considered. **c**, Modelling of the response time versus thickness, considering both transport and capacitance, for a range of dielectric constant and mobility. Orange circles show the minimum achievable response time for each pair of dielectric constant and mobility. **d**, Simulated efficiency over response time for

a range of absorption coefficients from 2×10^3 to $1.1 \times 10^4 \text{ cm}^{-1}$. In this modelling, both capacitance and transport limitations are considered, but internal quantum efficiency is assumed to be independent of the thickness and constant at 1. **e**, Overlay of calculated response time of a photodetector versus device area for a range of mobility. When the transport becomes dominant in determining the response time, the trend is flattened. **f**, Modelled fall time (τ_f) over rise time (τ_r) for a photodetector with a range of indicated fall time ($\tau_r = 10 \mu\text{s}$ to 100 ps), in response to a light pulse of different duration. EQE, external quantum efficiency.

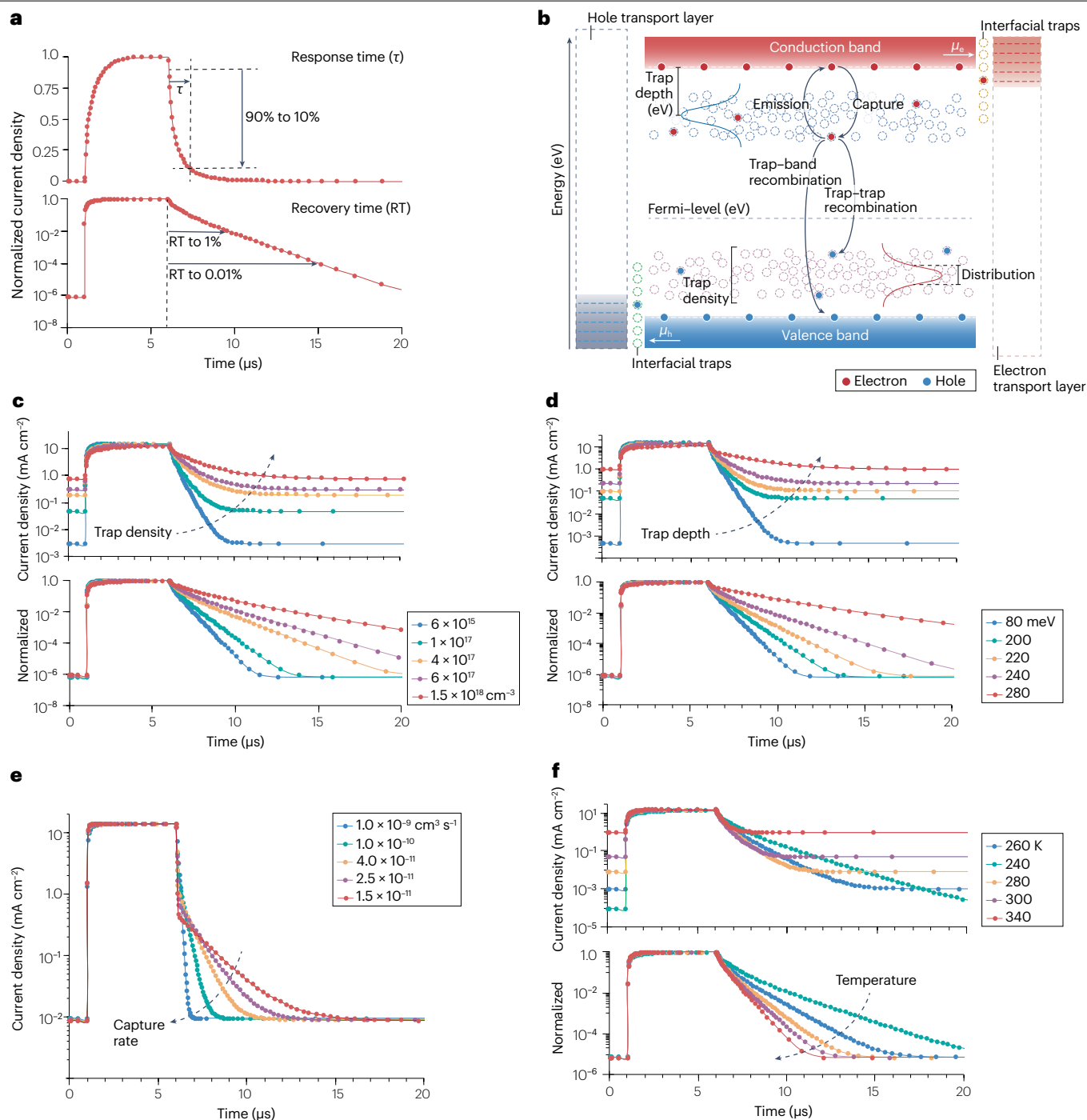


Fig. 4 | Trap-dictated RT. **a**, Comparison of response time (τ) and recovery time (RT): the photodetector's response to pulsed light is presented in both linear and logarithmic scales. **b**, A representation of the trap characteristics, along with the associated pathways for the capture, emission and recombination of electron traps. **c–f**, The simulated response to a 5- μ s pulsed light, in the presence

of electron traps within the specified range of trap density (panel c), trap depth (panel d), capture rate coefficient (panel e) and temperature (panel f). For each panel, all parameters remain constant with the exception of the indicated variable. Recombination possibility through the traps has not been factored into these simulations. μ , mobility. Simulations done using SETFOS software.

Traps can be positioned at different energies within the bandgap, where charge carriers might settle^{44–47}. From a device perspective, traps can originate from the active layer (atomic vacancies, interstitials

and dislocations; dopants and impurities; and grain boundaries in polycrystalline materials) or stem from the different junctions and interfaces (lattice mismatch, dangling bonds and surface states)

across the device. The Shockley–Read–Hall (SRH) model quantitatively describes these traps and their implications⁴⁸. The model suggests that electrons and holes can be captured, released (emitted) and recombined through both electron and hole traps (Fig. 4b). Given that trapped charge carriers have extended lifetimes relative to the transit time of free carriers, the recovery time is predominantly influenced by the slow release of these trapped carriers.

Trap dynamic modelling

Traps in semiconductor materials can be characterized by three main parameters: capture rate, trap density and trap depth. Focusing on electron traps, the capture rate (R_c) is determined by the rate at which electrons are captured from the conduction band by traps⁴⁸, expressed as

$$R_c = c_n n N_{t0} \quad (3)$$

where n represents the free electron concentration in the conduction band, N_{t0} the density of unoccupied electron trap states and c_n the electron capture rate coefficient. According to the SRH model, if the speed of the electron (typically thermal velocity) is v and the cross-section for capture by a trap is σ , then we have $c_n = \sigma v$. Here, σ is the cross-section through which an electron must pass to be captured, and it may be related to charge carrier mobility, applied field and temperature.

Considering only the capture and emission via electron traps, the dynamics of trapped carriers can be expressed as:

$$dn_t/dt = \text{capture rate} - \text{emission rate} = [\sigma v n (N_t - n_t)] - [e_n n_t] \quad (4)$$

where n_t is the concentration of trapped carriers, e_n the frequency of emission and N_t the total density of trap states.

At equilibrium ($dn_t/dt = 0$), emission and capture rates are equal. By considering the Fermi–Dirac distribution function to calculate the probability of an electron occupying the trap energy level (E_t), the emission frequency can be estimated:

$$e_n = \sigma v N_c \exp(E_t - E_c/kT) \quad (5)$$

When the light is turned off, the number of free carriers drops rapidly, and trap emission becomes dominant. The lifetime of the trapped carrier can then be related to the emission frequencies: $\tau_{tr} = e_n^{-1}$ (ref. 49).

From the equations described above, it becomes clear that the capture rate has a direct effect on the lifetime of trapped carriers, which in turn affects the recovery time (Fig. 4e). Beyond influencing recovery time, traps have a pronounced effect on the dark current (baseline response in absence of the light). Traps serve as undesired recombination centres and create accessible states for charge injection from contacts, whether transport layers or electrodes, leading to small shunt resistances and deviations from ideal diode characteristics^{50–53}. N_t is determined by the number of trap sites available within a given energy in a unit area. In general, increasing N_t leads to increases in dark current and extended recovery times⁴² (Fig. 4c).

The effective release of charge carriers from a trap, and their emission to the conduction/valence bands, requires external energy inputs. This energy can be harnessed from the available thermal energy, enough to overcome the activation energy governed by the Arrhenius equation. This activation energy, called trap depth, is equivalent to the energy difference between the trap states and the corresponding transport band ($E_t - E_c$) in the context of electron traps). Deeper trap depths into the midgap lead to elongated recovery times and dark current (Fig. 4d). In the presence of a significant external electric field across the film, trapped carriers might be released by tunnelling or

hopping from the trap states, either into a transport band or resulting in trap-assisted transport^{54,55}.

Using temperature as a multilevel diagnosis tool

Analysing the influence of temperature on photodetector performance can provide insights into performance limitations related to its time response. For example, temperature can aid in charge release from deeper traps, reduce overall trap lifetime and improve recovery time. However, increases in temperature also increase charge recombination and tunnelling and/or hopping events, thereby amplifying dark current and noise level (Fig. 4f). Temperature plays a key role in thermal admittance spectroscopy, thermally stimulated current and deep-level transient spectroscopies, offering insights into the defect physics of materials such as trap depth and their density, distribution and capture cross-section^{35,56}. It also serves as an exceptional diagnostic tool for evaluating transport mechanisms, as each mechanism shows distinct temperature-dependent behaviour^{57–61}.

Beyond the SRH model

It should be noted that the SRH model assumes ideal crystalline systems, with a bandlike transport. These assumptions might not be adequate for disordered materials, where transport is not delocalized and bandlike, but proceeds through localized states and results in a low overall charge-carrier mobility. Polycrystalline and disordered materials will also have a non-uniform distribution of states in both the energy and space landscapes. Although the core principles of trap physics, statistics and dynamic modelling remain consistent across various materials, it is crucial to reassess the initial assumptions of the SRH model when adapting it to a specific material system in the complete device stack. An example is the adoption of the SRH model for disordered organic semiconductors, which are characterized by limited mobility and hopping transport between localized states^{45,59,62–65}.

Outlook and direction of development

With the target of maximizing the gain and speed characteristics, below we briefly discuss potential directions from the perspective of materials and device architecture.

Materials perspective

The exceptional mobility of 2D materials contributes to their combined efficiency and speed characteristics^{21–23,66–69}. To further enhance this aspect, focusing on increasing the absorption cross-section is advisable. This enhancement can be achieved through sophisticated light management (strategies to optimize the interaction of light and material) in the design of photodetector architecture^{70–75}. Exploring these meta-architectures in large pixel areas, which is crucial for some applications, and modulating their energetics in the bulk and at interfaces to reduce dark current and noise levels, could be interesting.

Organic materials have been recognized for their superior performance in minimizing dark current, but their limited mobility often results in a compromised response time²⁰. Recent studies, however, have demonstrated that organics can achieve high mobility, exceeding $1 \text{ cm}^2 \text{ V}^{-1} \text{ s}^{-1}$ (refs. 76–78). The development of organic, organometallic or polymeric materials that absorb in the infrared spectrum while maintaining high mobility presents a promising avenue for research.

Colloidal quantum dots (CQDs) are of interest in solution-processed fast infrared detectors, owing to their tunable properties. Despite their potential, they are often hampered by issues such as low stability and high dielectric constants, which limit their speed.

Recent advances in the development of III–V quantum-dot-based photodetectors, especially in the shortwave infrared region (in materials such as InAs), indicate a shift towards materials with more covalent characteristics, as opposed to conventional ionic PbS or CdS CQDs. This transition seems to mitigate previous limitations^{25,79–81}. In general, materials with a more covalent nature are advantageous; they not only reduce the dielectric constant and associated charging effects but are also less susceptible to ion motion and instability issues under external stimuli such as applied field or temperature. Continued investigation into the large-scale synthesis of monodisperse dots, the use of effective passivation schemes that include doping and energetic modifications, and the tailoring of transport layers within device architectures are critical for the development of solutions that could compete with current commercial technologies.

The progress in perovskite-based solar cells has direct implications for photodetection devices^{34,82–84}. Binary PbSn perovskites, in particular, have shown a favourable balance between efficiency and speed, especially for near-infrared (NIR) detection²⁰. The primary challenge with perovskites lies in the limitation of their bandgap to the visible and near-infrared region. Investigating new perovskite compositions and structures with a reduced bandgap is essential.

Device physics and architecture

To maximize the detection speed, architectures can be designed that use carrier transport mechanisms largely exempt from energy dissipation and scattering events, thus enabling near-instantaneous transport. Coherent tunnelling serves as a prime example of such a mechanism^{60,61}. This quantum mechanical phenomenon allows carriers to traverse transport barriers rather than surmount them classically. Given that the process does not depend on thermal activation and is immune to scattering, it operates in a nearly instantaneous, ballistic manner once the conditions for its occurrence are met. This brings advantages in both high-speed and temperature-independent operations, suitable for detection in extremely low temperatures⁸⁵. In this area, further research is needed in designing nanostructures that allow sequential tunnelling through a series of coupled metal–semiconductor assemblies or using on-chip waveguide platforms to establish light propagation pathways that are orthogonal to the tunnelling direction. An example involves expanding on the resonant (activationless) photostimulated current demonstrated in covalently bonded aromatic oligomers^{85,86} and their integration into a hybrid waveguide platform. This approach can markedly increase light absorption while keeping the excited carrier tunnelling distance under 10 nm.

Advancing and integrating quenching mechanisms for high-gain devices is another promising avenue. In situations involving short-pulsed light measurement, once the peak response is reached, additional signal amplification through the gain mechanism becomes adverse. Quenching the recirculation of carriers, either optically or electrically, can substantially enhance the achievable speed of the device. Such a quenching mechanism would be particularly advantageous for the development of high-speed photoconductors. This concept could greatly benefit from insights gleaned from the mature techniques used in passive and active response quenching for avalanche and single-photon detectors^{87–90}.

Light management strategies, particularly in devices featuring materials with low mobility (like organic materials) and a small absorption cross-section (such as 2D materials), are used to increase the EQE of devices. However, these strategies can be repurposed to maximize the speed of detection. Making use of the high travel speed of light,

nanometric quantum wells (confined spaces for the recirculation of light) can be designed to minimize the carrier transit time while EQE is not compromised.

Decoupling the absorption from the carrier transport and multiplication processes offers a strategic pathway for optimizing photodetector performance. Platforms such as avalanche photodetectors have already benefited from such decoupling. More opportunities exist to delve deeper into probe structures, architectures and detection principles. The primary objective is to enhance gains without sacrificing speed or elevating the dark current, especially when integrating multiple components in photonic systems²⁶. In this realm, a diverse class of materials can be integrated in a manner that leverages their individual strengths, leading to optimized device performance. Two main approaches are emerging for this decoupling. The first is the innovative design of detector architectures that allows for the integration of different layers with distinct roles. For instance, one can implement hybrid photo-FET architectures by pairing high-mobility 2D materials (which serve as the transport layer) with colloidal quantum dots as active layers having tunable absorption characteristics. The second is a method wherein hybrid materials are purposely constructed to maximize their synergistic functionality. For instance, one can imagine vertically aligned 2D perovskites with double-sided anchoring cations that bridge the perovskite quantum wells to an organic layer that absorbs infrared light. Such a design has the potential for fast and tunable infrared detection.

Emphasizing the investigation of trap origins and devising strategies to reduce their density and depth, both at the synthesis and device (interfaces) levels, are instrumental in improving the recovery time. Yet controlling and tuning these parameters, especially in solution-processed materials, presents considerable challenges. Where recovery time acts as a bottleneck, a stimulated detrapping mechanism could prove advantageous. For example, a secondary light pulse with energy equal to the trap depth, following the main pulse, can stimulate the emission of trapped charges into the corresponding energy band, followed by their rapid extraction through the contacts. As the energy of these complementary pulses is below the material's bandgap, they do not induce excitation from ground states. Given that the flux of these emitted charges is relatively low compared with the main peak (small cross-section), the population of the recaptured charges is negligible. We note that the integration of these de-trapping mechanisms, which incur additional costs to the system, must be evaluated in terms of total cost efficiency. For practicality, the assessment should be made in comparison to existing solutions for the intended applications, ensuring that the added expense is justified by the performance improvements or benefits.

Published online: 22 March 2024

References

1. Eng, P. C., Song, S. & Ping, B. State-of-the-art photodetectors for optoelectronic integration at telecommunication wavelength. *Nanophotonics* **4**, 277–302 (2015).
2. Pelucchi, E. et al. The potential and global outlook of integrated photonics for quantum technologies. *Nat. Rev. Phys.* **4**, 194–208 (2022).
3. Moody, G. et al. Roadmap on integrated quantum photonics. *J. Phys. Photonics* **4**, 012501 (2022).
4. Madsen, L. S. et al. Quantum computational advantage with a programmable photonic processor. *Nature* **606**, 75–81 (2022).
5. Li, N. et al. A progress review on solid-state LiDAR and nanophotonics-based LiDAR sensors. *Laser Photonics Rev.* **16**, 2100511 (2022).
6. Kim, I. et al. Nanophotonics for light detection and ranging technology. *Nat. Nanotechnol.* **16**, 508–524 (2021).
7. Huseynzade, K., Sadigov, A. & Naghiyev, J. in *4th Int. Conf. Artificial Intelligence Applied Mathematics Engineering* (eds Hemanth, D. J. et al.) 680–690 (Springer, 2023).
8. Goossens, S., Konstantatos, G. & Oikonomou, A. Colloidal quantum dot image sensors: technology and marketplace opportunities. *Inf. Disp.* **37**, 18–23 (2021).

9. Lee, J. et al. Imaging in short-wave infrared with 1.82 μm pixel pitch quantum dot image sensor (IEDM, 2020).
10. Gregory, C., Hilton, A., Violette, K. & Klem, E. J. D. Colloidal quantum dot photodetectors for large format NIR, SWIR, and ESWIR imaging arrays. *SID Int. Symp. Dig. Tech. Pap.* **52**, 982–986 (2021).
11. Jiang, Y., Karpf, S. & Jalali, B. Time-stretch LiDAR as a spectrally scanned time-of-flight ranging camera. *Nat. Photonics* **14**, 14–18 (2020).
12. Li, N., Hu, X., Sui, X., Chen, Q. & Ng, T. N. Infrared light detection technology based on organics. *ACS Appl. Electron. Mater.* **5**, 21–33 (2023).
13. Shan, T., Hou, X., Yin, X. & Guo, X. Organic photodiodes: device engineering and applications. *Front. Optoelectron.* **15**, 49 (2022).
14. Wang, Y. et al. Narrowband organic photodetectors — towards miniaturized, spectroscopic sensing. *Mater. Horiz.* **9**, 220–251 (2022).
15. Ren, H., Chen, J. D., Li, Y. Q. & Tang, J. X. Recent progress in organic photodetectors and their applications. *Adv. Sci.* **8**, 2002418 (2021).
16. Liu, J. et al. Challenges and recent advances in photodiodes-based organic photodetectors. *Mater. Today* **51**, 475–503 (2021).
17. Xu, Q. et al. Ultrafast colloidal quantum dot infrared photodiode. *ACS Photonics* **7**, 1297–1303 (2020).
18. Vafaie, M. et al. Colloidal quantum dot photodetectors with 10-ns response time and 80% quantum efficiency at 1,550 nm. *Matter* **4**, 1042–1053 (2021).
19. Nakotte, T. et al. Colloidal quantum dot based infrared detectors: extending to the mid-infrared and moving from the lab to the field. *J. Mater. Chem. C* **10**, 790–804 (2022).
20. Morteza Najarian, A. et al. Sub-millimetre light detection and ranging using perovskites. *Nat. Electron.* **5**, 511–518 (2022).
21. Kufer, D. & Konstantatos, G. Photo-FETs: phototransistors enabled by 2D and OD nanomaterials. *ACS Photonics* **3**, 2197–2210 (2016).
22. Khan, S. et al. 2D heterostructures for highly efficient photodetectors: from advanced synthesis to characterizations, mechanisms, and device applications. *Adv. Photonics Res.* **3**, 2100342 (2022).
23. Liu, C. et al. Silicon/2D-material photodetectors: from near-infrared to mid-infrared. *Light Sci. Appl.* **10**, 123 (2021).
24. García de Arquer, F. P. et al. Semiconductor quantum dots: technological progress and future challenges. *Science* **373**, eaaz8541 (2021).
25. Sun, B. et al. Fast near-infrared photodetection using III–V colloidal quantum dots. *Adv. Mater.* **34**, 2203039 (2022).
26. Konstantatos, G. Current status and technological prospect of photodetectors based on two-dimensional materials. *Nat. Commun.* **9**, 5266 (2018).
27. Wang, J., Sciarrino, F., Laing, A. & Thompson, M. G. Integrated photonic quantum technologies. *Nat. Photonics* **14**, 273–284 (2020).
28. Giordani, T., Hoch, F., Carvacho, G., Spagnolo, N. & Sciarrino, F. Integrated photonics in quantum technologies. *Riv. Nuovo Cimento* **46**, 71–103 (2023).
29. Elshaari, A. W., Pernice, W., Srinivasan, K., Benson, O. & Zwiller, V. Hybrid integrated quantum photonic circuits. *Nat. Photonics* **14**, 285–298 (2020).
30. Luo, W. et al. Recent progress in quantum photonic chips for quantum communication and internet. *Light Sci. Appl.* **12**, 175 (2023).
31. Gyger, S. et al. Reconfigurable photonics with on-chip single-photon detectors. *Nat. Commun.* **12**, 1408 (2021).
32. Fang, H., Hu, W., Fang, H. & Hu, W. Photogating in low dimensional photodetectors. *Adv. Sci.* **4**, 1700323 (2017).
33. Shi, J., Li, D., Luo, Y., Wu, H. & Meng, Q. Opto-electro-modulated transient photovoltage and photocurrent system for investigation of charge transport and recombination in solar cells. *Rev. Sci. Instrum.* **87**, 123107 (2016).
34. Gong, S. et al. Ultrafast dynamics in perovskite-based optoelectronic devices. *Cell Rep. Phys. Sci.* **4**, 101580 (2023).
35. Srivastava, S. et al. Advanced spectroscopic techniques for characterizing defects in perovskite solar cells. *Commun. Mater.* **4**, 52 (2023).
36. Lafalce, E., Zhang, C., Liu, X. & Vardeny, Z. V. Role of intrinsic ion accumulation in the photocurrent and photocapacitive responses of MAPbBr₃ photodetectors. *ACS Appl. Mater. Interfaces* **8**, 35447–35453 (2016).
37. Maier, A. et al. Sub-nanosecond intrinsic response time of PbS nanocrystal IR-photodetectors. *Nano Lett.* **22**, 2809–2816 (2022).
38. Shi, J. et al. From ultrafast to ultraslow: charge-carrier dynamics of perovskite solar cells. *Joule* **2**, 879–901 (2018).
39. Wang, Q., Moser, J. E. & Grätzel, M. Electrochemical impedance spectroscopic analysis of dye-sensitized solar cells. *J. Phys. Chem. B* **109**, 14945–14953 (2005).
40. Rossi, F. & Kuhn, T. Theory of ultrafast phenomena in photoexcited semiconductors. *Rev. Mod. Phys.* **74**, 895–950 (2002).
41. Bisquert, J. Theory of the impedance of electron diffusion and recombination in a thin layer. *J. Phys. Chem. B* **106**, 325–333 (2002).
42. Wu, Z. et al. Noise and detectivity limits in organic shortwave infrared photodiodes with low disorder. *npj Flex. Electron.* **4**, 6 (2020).
43. Fang, Y., Armin, A., Meredith, P. & Huang, J. Accurate characterization of next-generation thin-film photodetectors. *Nat. Photonics* **13**, 1–4 (2019).
44. Ma, X., Janssen, R. A. J. & Gelincik, G. H. Trap-assisted charge generation and recombination in state-of-the-art organic photodetectors. *Adv. Mater. Technol.* **8**, 2300234 (2023).
45. Ndiaye, N. S., Simonetti, O., Nguyen, T. P. & Giraudet, L. Generation-recombination in disordered organic semiconductor: application to the characterization of traps. *Org. Electron.* **99**, 106350 (2021).
46. Bao, C. & Gao, F. Physics of defects in metal halide perovskites. *Rep. Prog. Phys.* **85**, 096501 (2022).
47. Kao, K. C. in *Dielectric Phenomena in Solids* Ch. 7 (Academic, 2004).
48. Shockley, W. & Read, W. T. Statistics of the recombinations of holes and electrons. *Phys. Rev.* **87**, 835–842 (1952).
49. Konstantatos, G. & Sargent, E. H. PbS colloidal quantum dot photoconductive photodetectors: transport, traps, and gain. *Appl. Phys. Lett.* **91**, 100–102 (2007).
50. Zarrabi, N. et al. Charge-generating mid-gap trap states define the thermodynamic limit of organic photovoltaic devices. *Nat. Commun.* **11**, 5567 (2020).
51. Ahmadi, M., Wu, T. & Hu, B. A review on organic–inorganic halide perovskite photodetectors: device engineering and fundamental physics. *Adv. Mater.* **29**, 1605242 (2017).
52. Kublitski, J. et al. Reverse dark current in organic photodetectors and the major role of traps as source of noise. *Nat. Commun.* **12**, 551 (2021).
53. Simone, G., Dyson, M. J., Meskers, S. C. J., Janssen, R. A. J. & Gelincik, G. H. Organic photodetectors and their application in large area and flexible image sensors: the role of dark current. *Adv. Funct. Mater.* **30**, 1904205 (2020).
54. Ollearo, R. et al. Ultralow dark current in near-infrared perovskite photodiodes by reducing charge injection and interfacial charge generation. *Nat. Commun.* **12**, 7277 (2021).
55. Furlan, J. Tunneling generation-recombination currents in a-Si junctions. *Prog. Quantum Electron.* **25**, 55–96 (2001).
56. Bozyigit, D. & Wood, V. Electrical characterization of nanocrystal solids. *J. Mater. Chem. C* **2**, 3172–3184 (2014).
57. Neamen, D. Semiconductor physics and devices. *Mater. Today* **9**, 57 (2006).
58. Kasap, S. O. *Principles of Electronic Materials and Devices* 4th edn (McGraw-Hill Education, 2018).
59. Bässler, H. & Köhler, A. in *Unimolecular and Supramolecular Electronics I. Topics in Current Chemistry* Vol. 312 (ed. Metzger, R.) 1–65 (Springer, 2011).
60. McCreery, R. L. Carbon-based molecular junctions for practical molecular electronics. *Acc. Chem. Res.* **55**, 2766–2779 (2022).
61. Morteza Najarian, A. & McCreery, R. L. Structure controlled long-range sequential tunneling in carbon-based molecular junctions. *ACS Nano* **11**, 3542–3552 (2017).
62. Nenashev, A. V., Oelerich, J. O. & Baranovskii, S. D. Theoretical tools for the description of charge transport in disordered organic semiconductors. *J. Phys. Condens. Matter* **27**, 093201 (2015).
63. Baranovskii, S. D. Theoretical description of charge transport in disordered organic semiconductors. *Phys. Status Solidi B* **251**, 487–525 (2014).
64. Kuik, M., Koster, L. J. A., Wetzelaer, G. A. H. & Blom, P. W. M. Trap-assisted recombination in disordered organic semiconductors. *Phys. Rev. Lett.* **107**, 256805 (2011).
65. Tessler, N., Preezant, Y., Rappaport, N. & Roichman, Y. Charge transport in disordered organic materials and its relevance to thin-film devices: a tutorial review. *Adv. Mater.* **21**, 2741–2761 (2009).
66. Cheng, L., Zhang, C. & Liu, Y. The optimal electronic structure for high-mobility 2D semiconductors: exceptionally high hole mobility in 2D antimony. *J. Am. Chem. Soc.* **141**, 16296–16302 (2019).
67. Zhang, K. et al. Recent progress and challenges based on two-dimensional material photodetectors. *Nano Express* **2**, 012001 (2021).
68. Yan, F. et al. Toward high-performance photodetectors based on 2D materials: strategy on methods. *Small Methods* **2**, 1700349 (2018).
69. Malik, M., Iqbal, M. A., Choi, J. R. & Pham, P. V. 2D materials for efficient photodetection: overview, mechanisms, performance and UV-IR range applications. *Front. Chem.* **10**, 905404 (2022).
70. Wang, J., Han, J., Chen, X. & Wang, X. Design strategies for two-dimensional material photodetectors to enhance device performance. *InfoMat* **1**, 33–53 (2019).
71. Kwak, D., Polyushkin, D. K. & Mueller, T. In-sensor computing using a MoS₂ photodetector with programmable spectral responsivity. *Nat. Commun.* **14**, 4264 (2023).
72. Amani, M. et al. Solution-synthesized high-mobility tellurium nanoflakes for short-wave infrared photodetectors. *ACS Nano* **12**, 7253–7263 (2018).
73. Tan, C. et al. Evaporated Se_xTe_{1-x} thin films with tunable bandgaps for short-wave infrared photodetectors. *Adv. Mater.* **32**, 2001329 (2020).
74. Yu, X. et al. Atomically thin noble metal dichalcogenide: a broadband mid-infrared semiconductor. *Nat. Commun.* **9**, 1545 (2018).
75. Sefidmooye Azar, N. et al. Long-wave infrared photodetectors based on 2D platinum diselenide atop optical cavity substrates. *ACS Nano* **15**, 6573–6581 (2021).
76. Shuai, Z., Geng, H., Xu, W., Liao, Y. & André, J. M. From charge transport parameters to charge mobility in organic semiconductors through multiscale simulation. *Chem. Soc. Rev.* **43**, 2662–2679 (2014).
77. Ghorab, M., Fattah, A. & Joodaki, M. Fundamentals of organic solar cells: a review on mobility issues and measurement methods. *Optik* **267**, 169730 (2022).
78. Shaw, J. M. & Seidler, P. F. Organic electronics: introduction. *IBM J. Res. Dev.* **45**, 3–8 (2001).
79. Vafaie, M. et al. Molecular surface programming of rectifying junctions between InAs colloidal quantum dot solids. *Proc. Natl Acad. Sci. USA* **120**, e2305327120 (2023).
80. Xia, P. et al. Sequential co-passivation in InAs colloidal quantum dot solids enables efficient near-infrared photodetectors. *Adv. Mater.* **35**, 2301842 (2023).
81. Xia, P. et al. Arresting ion migration from the ETL increases stability in infrared light detectors based on III–V colloidal quantum dots. *Adv. Mater.* **36**, 2310122 (2023).
82. Jokar, E., Cai, L., Han, J., Nacpil, E. J. C. & Jeon, I. Emerging opportunities in lead-free and lead-tin perovskites for environmentally viable photodetector applications. *Chem. Mater.* **35**, 3404–3426 (2023).

83. Liu, F. et al. Highly efficient and stable self-powered mixed tin–lead perovskite photodetector used in remote wearable health monitoring technology. *Adv. Sci.* **10**, 2205879 (2023).
84. Wang, H. et al. A review of perovskite-based photodetectors and their applications. *Nanomaterials* **12**, 4390 (2022).
85. Najarian, A. M. & McCreery, R. L. Long-range activationless photostimulated charge transport in symmetric molecular junctions. *ACS Nano* **13**, 867–877 (2019).
86. Morteza Najarian, A., Bayat, A. & McCreery, R. L. Orbital control of photocurrents in large area all-carbon molecular junctions. *J. Am. Chem. Soc.* **140**, 1900–1909 (2018).
87. Zheng, J. et al. Dynamic-quenching of a single-photon avalanche photodetector using an adaptive resistive switch. *Nat. Commun.* **13**, 1517 (2022).
88. Cova, S., Ghioni, M., Lacaíta, A., Samori, C. & Zappa, F. Avalanche photodiodes and quenching circuits for single-photon detection. *Appl. Opt.* **35**, 1956 (1996).
89. Tisa, S., Guerrieri, F. & Zappa, F. Variable-load quenching circuit for single-photon avalanche diodes. *Opt. Express* **16**, 2232 (2008).
90. Bronzi, D. et al. Fast sensing and quenching of CMOS SPADs for minimal afterpulsing effects. *IEEE Photonics Technol. Lett.* **25**, 776–779 (2013).
91. Xu, Y. & Lin, Q. Photodetectors based on solution-processable semiconductors: recent advances and perspectives. *Appl. Phys. Rev.* **7**, 11315 (2020).
92. Harter, A. C., Tabbert, B. & Goushcha, O. in *Proc. SPIE 10526 Physics Simulation Optoelectronic Devices XXVI* (SPIE, 2018).
93. Saran, R. & Curry, R. J. Lead sulphide nanocrystal photodetector technologies. *Nat. Photonics* **10**, 81–92 (2016).
94. Villa, F., Severini, F., Madonini, F. & Zappa, F. SPADs and SiPMs arrays for long-range high-speed light detection and ranging (lidar). *Sensors* **21**, 3839 (2021).
95. Liu, H. D. et al. Avalanche photodiode punch-through gain determination through excess noise analysis. *J. Appl. Phys.* **106**, 64507 (2009).
96. Kang, Y. et al. Monolithic germanium/silicon avalanche photodiodes with 340GHz gain–bandwidth product. *Nat. Photonics* **3**, 59–63 (2009).
97. Kleinow, P. et al. Charge-layer design considerations in SAGCM InGaAs/InAlAs avalanche photodiodes. *Phys. Status Solidi Appl. Mater. Sci.* **213**, 925–929 (2016).
98. García de Arquer, F. P., Armin, A., Meredith, P. & Sargent, E. H. Solution-processed semiconductors for next-generation photodetectors. *Nat. Rev. Mater.* **2**, 16100 (2017).
99. Adinolfi, V. & Sargent, E. H. Photovoltage field-effect transistors. *Nature* **542**, 324–327 (2017).
100. Neubauer, A., Yochelis, S., Amit, Y., Banin, U. & Paltiel, Y. Highly sensitive room temperature infrared hybrid organic–nanocrystal detector. *Sens. Actuators A* **229**, 166–171 (2015).
101. Aqua, T., Naaman, R., Aharoni, A., Banin, U. & Paltiel, Y. Hybrid nanocrystals–organic–semiconductor light sensor. *Appl. Phys. Lett.* **92**, 223112 (2008).

Acknowledgements

F.P.G.A. acknowledges support from CEX2019-000910-S (MCIN/AEI/10.13039/501100011033), Fundació Cellex and Mir-Puig; from Generalitat de Catalunya through CERCA; and from the La Caixa Foundation (100010434, EU Horizon 2020 Marie Skłodowska-Curie grant agreement 847648).

Author contributions

All authors contributed equally to this manuscript.

Competing interests

The authors declare no competing interests.

Additional information

Peer review information *Nature Reviews Physics* thanks Zhijun Ning and the other, anonymous, reviewer(s) for their contribution to the peer review of this work.

Publisher's note Springer Nature remains neutral with regard to jurisdictional claims in published maps and institutional affiliations.

Springer Nature or its licensor (e.g. a society or other partner) holds exclusive rights to this article under a publishing agreement with the author(s) or other rightsholder(s); author self-archiving of the accepted manuscript version of this article is solely governed by the terms of such publishing agreement and applicable law.

Related links

SETFOS software: <https://www.fluxim.com/setfos-intro>

© Springer Nature Limited 2024